

Tunneling chirality Hall effect in type-I Weyl semimetals

W. Zeng ^{*}*Department of Physics, Jiangsu University, Zhenjiang 212013, China*

(Received 25 April 2024; revised 18 June 2024; accepted 10 July 2024; published 18 July 2024)

We propose a tilt-assisted tunneling chirality Hall effect in the normal metal-superconductor (NS) junctions based on the time-reversal-broken type-I Weyl semimetals. It is found that the chirality-dependent skew reflection occurs at the NS interface due to the tilt of the Weyl cones, which is responsible for the nonzero transverse chirality Hall currents. Distinct from the Hall effect induced by the Berry curvature, we further illustrate that the transverse chirality current here is determined by the symmetry of the tilted Weyl Hamiltonian. Specifically, both the transverse chirality Hall current and the transverse charge Hall current may occur when the tilt of the Weyl cones break the mirror symmetry (\mathcal{M}) of the Weyl Hamiltonian. However, a pure transverse chirality Hall current with zero net charge is present when the tilt breaks \mathcal{M} symmetry but preserves the combined \mathcal{MC} symmetry, where \mathcal{C} represents the \mathbb{Z}_2 exchange symmetry.

DOI: [10.1103/PhysRevB.110.024511](https://doi.org/10.1103/PhysRevB.110.024511)

I. INTRODUCTION

Weyl semimetals are three-dimensional topological materials with the conduction and valence bands touching at two or more crossing points in the bulk, which are known as the Weyl nodes [1–3]. The emergence of the nontrivial and stable Weyl nodes requires the breaking of either time-reversal symmetry (\mathcal{T}) or spatial inversion symmetry (\mathcal{I}). As a consequence of the Nielsen-Ninomiya theorem [4], the minimal model of the \mathcal{T} symmetry-broken Weyl semimetal contains a single pair of Weyl nodes, whereas the \mathcal{I} symmetry-broken one contains four Weyl nodes [5,6]. Each of the paired Weyl nodes acts like a topological charge with the charge sign corresponding to its chirality [7,8]. The manipulation of the chirality is one of the hot topics in Weyl physics. Up to now, several works have been devoted to such chirality-dependent physics of Weyl semimetals, such as the chiral anomaly [9–11], chirality-dependent Hall effect [12–14], and chirality Josephson effect [15,16].

A finite tilt of the Weyl cones can be generated because the Lorentz symmetry is not necessarily the symmetry group in condensed matter systems [17]. Distinct from the graphene-like materials where the tilting is usually weak [18–20], the tilting can be strong in Weyl semimetals. Depending on whether the Weyl cone is overtilted or not, Weyl semimetals can be classified into two subgroups, i.e., type-I and type-II Weyl semimetals [21–24]. The type-I Weyl semimetals possess a closed Fermi surface enclosing either an electron or a hole pocket, with a vanishing density of states at the Weyl nodes. The type-II Weyl semimetals host overtilted Weyl cones and the Fermi surface near the Weyl nodes is hyperboloidal with a large density of states, leading to the electron and hole pockets near the Weyl nodes [25,26]. Many tilt-induced intriguing transport properties have been reported in

Weyl semimetals, such as the anomalous Nernst and thermal Hall effects [27], double Andreev reflection [28], tilt-assisted π -phase Josephson current [29], and linear magnetochiral transport [30].

A very recent interesting work [31] reported that the tilt mechanism can lead to the tunneling valley Hall effect in Dirac systems, where a strong tilt-dependent transverse valley Hall current can be generated by the momentum filtering of the tunneling Dirac fermions. Subsequently, the nonlinear valley Hall effect in tilted massless Dirac fermions in strained graphene and organic semiconductors was predicted [32]. Inspired by this, here we propose a tilt-induced tunneling chirality Hall effect in Weyl semimetals. We theoretically investigate the transverse charge and chirality transport in the normal metal-superconductor (NS) junctions based on the type-I Weyl semimetals, which breaks the time-reversal symmetry but preserves the inversion symmetry. It is found that the scattering at the NS interface is chirality dependent. For the electrons with a given chirality, the incident-angle-resolved reflection probability is asymmetric, which is responsible for the transverse chirality Hall current. The chirality Hall conductance arising from the skew scattering can be obtained within the Landauer formalism [33]. We further demonstrate that the transverse chirality Hall current here is related to the symmetry of the tilted Weyl Hamiltonian, and determined by the intersection angle between the line connecting the two opposite chiral Weyl nodes and the normal of the NS interface. Specifically, for the tilt breaking the mirror symmetry \mathcal{M} , both the transverse chirality Hall current and charge Hall current may occur. However, for the tilt breaking the \mathcal{M} symmetry but preserving the combined \mathcal{MC} symmetry with \mathcal{C} being the \mathbb{Z}_2 exchange symmetry, a pure transverse chirality Hall current with zero net charge appears.

The remainder of the paper is organized as follows. The model Hamiltonian and the scattering approach are explained in detail in Sec. II. The numerical results and discussions are presented in Sec. III. Finally, we conclude in Sec. IV.

*Contact author: zeng@ujs.edu.cn

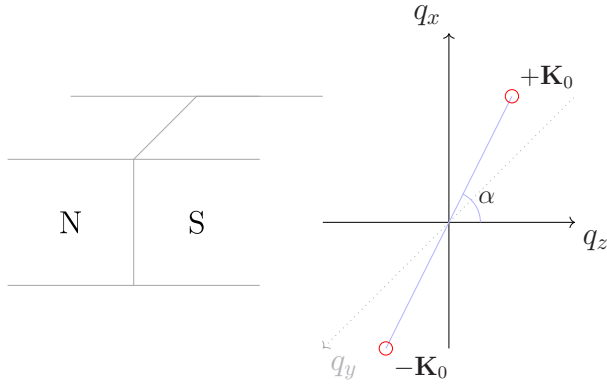


FIG. 1. (Left) Sketch of the NS junction under consideration, where the normal of the NS interface is along the z axis. (Right) Schematic of the momentum space with two Weyl nodes at momenta $\pm\mathbf{K}_0$. The angle between the line connecting two Weyl nodes and the q_z axis is denoted by α .

II. MODEL

We consider the type-I Weyl semimetals-based NS junction along the z axis, where the normal and superconducting regions are located at $z < 0$ and $z > 0$, respectively, as shown in Fig. 1. Two opposite chiral Weyl nodes are situated at $\pm\mathbf{K}_0$ in the q_x - q_z plane, and the line connecting $\pm\mathbf{K}_0$ can make an angle of α with q_z axis. In the crystal coordinates, the minimal model for the type-I Weyl semimetal is described by the effective two-band Hamiltonian [34,35]

$$H = \sum_{\chi, \mathbf{q}} \Psi_{\chi, \mathbf{q}}^\dagger \mathcal{H}_\chi(\mathbf{q}) \Psi_{\chi, \mathbf{q}}, \quad (1)$$

where $\Psi_{\chi, \mathbf{q}} = (\psi_{\chi, \mathbf{q}\uparrow}, \psi_{\chi, \mathbf{q}\downarrow})^T$ is the spinor basis with $\chi = \pm$ being the chirality of the Weyl nodes and $\mathbf{q} = (q_1, q_2, q_3)$ is the momentum measured from $\chi\mathbf{K}_0$. Around the Weyl nodes, the low-energy Hamiltonian reads [29,36]

$$\mathcal{H}_\chi(\mathbf{q}) = \hbar v_\chi q_1 \sigma_0 + \hbar v_F (q_1 \sigma_1 + q_2 \sigma_2 - \chi q_3 \sigma_3), \quad (2)$$

where v_F is the Fermi velocity, σ_0 is the identity matrix, and σ_i ($i = 1, 2, 3$) are Pauli matrices acting on the spin space. The tilt of the Weyl cones is along the q_1 direction with the parameter v_χ . Here we focus on the tilting effect in the type-I Weyl semimetals, i.e., $|v_\chi| < v_F$. The inversion symmetry of the Hamiltonian in Eq. (2) requires $\sigma_3 \mathcal{H}_+(\mathbf{q}) \sigma_3 = \mathcal{H}_(-\mathbf{q})$, leading to $v_+ = -v_-$, which implies that the opposite chiral Weyl cones have tilts in opposite directions. It is convenient to work with the junction coordinates, where the transport direction is assumed to be along the z axis, as shown in Fig. 1. The two different coordinate systems are related by the rotation transformation

$$\begin{aligned} q_1 &= q_x \cos \alpha - q_z \sin \alpha, & q_2 &= q_y, \\ q_3 &= q_z \cos \alpha + q_x \sin \alpha, \end{aligned} \quad (3)$$

where α is the angle between the line connecting two Weyl nodes and the q_z axis. Similarly, the spin-1/2 Pauli matrices in the crystal coordinate system and the junction coordinate system, denoted by $\sigma_{1,2,3}$ and $\sigma_{x,y,z}$, respectively, are related by the same rotation transformation

$$\begin{aligned} \sigma_1 &= \sigma_x \cos \alpha - \sigma_z \sin \alpha, & \sigma_2 &= \sigma_y, \\ \sigma_3 &= \sigma_z \cos \alpha + \sigma_x \sin \alpha. \end{aligned} \quad (4)$$

In the superconducting region, the zero-momentum BCS pairing is preferred for inversion-symmetric Weyl semimetals [37], for which the paired electrons are from two Weyl nodes with opposite chirality. This BCS superconductivity can be induced by the conventional superconductor via the proximity effect in the Weyl semimetal-based junction [34,38]. The pairing Hamiltonian reads

$$\mathcal{H}_\Delta = \sum_{\chi, s} \int d\mathbf{r} \Delta \psi_{\chi, s}^\dagger(\mathbf{r}) \psi_{-\chi, -s}^\dagger(\mathbf{r}) + \text{H.c.}, \quad (5)$$

where $s = \{\uparrow, \downarrow\}$ is the spin index and Δ is the pairing potential. In the Nambu basis $(\psi_{\chi\uparrow}, \psi_{\chi\downarrow}, \psi_{-\chi\downarrow}^\dagger, -\psi_{-\chi\uparrow}^\dagger)^T$, the NS junction is described by the Bogoliubov–de Gennes (BdG) Hamiltonian [39–41]

$$\mathcal{H}_{BdG} = \begin{pmatrix} \mathcal{H}_\chi(-i\nabla - \chi\mathbf{K}_0) - \mu(z) & \Delta(z) \\ \Delta^*(z) & \mu(z) - \sigma_y \mathcal{H}_{-\chi}^*(-i\nabla + \chi\mathbf{K}_0) \sigma_y \end{pmatrix}, \quad (6)$$

where the chemical potential $\mu(z) = \mu$ for $z < 0$ and $\mu(z) = \mu_s$ for $z > 0$, the pairing term $\Delta(z) = 0$ for $z < 0$, and $\Delta(z) = \Delta_0$ for $z > 0$. We first perform the gauge transformation $D = \exp(i\chi\mathbf{K}_0 \cdot \mathbf{r})$ which removes the large momentum \mathbf{K}_0 in the BdG Hamiltonian Eq. (6). Then we perform an extra unitary transformation $U = \sigma_x \exp(i\alpha\sigma_y)$ to remove the angle α from the hole part of the BdG Hamiltonian [15,29]. After performing U , the BdG Hamiltonian reads

$$\mathcal{H}_{BdG} = \begin{pmatrix} \hbar v_F (\chi c q_1 \sigma_0 + (q_x \sigma_x - \chi q_y \sigma_y + q_z \sigma_z)) - \mu(z) & \Delta_B(z) \\ \Delta_B(z) & \hbar v_F (-\chi c q_1 \sigma_0 - (q_x \sigma_x + \chi q_y \sigma_y + q_z \sigma_z)) + \mu(z) \end{pmatrix}, \quad (7)$$

where $c = |v_\chi/v_F|$ is a dimensionless parameter employed here to characterize the tilt ($0 < c < 1$), $q_i = q_x \cos \alpha - q_z \sin \alpha$, and $\Delta_B(z) = -\Delta(z) \sin \alpha \sigma_z + \Delta(z) \cos \alpha \sigma_x$.

In the normal segment of the junction ($z < 0$), the scattering states propagating along the $+z$ axis are given by

$$|\varphi_e^>\rangle = \begin{pmatrix} \Gamma_e^> \\ |\mathbf{q}_\parallel| e^{-i\phi} \\ 0 \\ 0 \end{pmatrix} e^{iq_e^> z}, \quad |\varphi_h^>\rangle = \begin{pmatrix} 0 \\ 0 \\ \Gamma_h^> \\ |\mathbf{q}_\parallel| e^{i\phi} \end{pmatrix} e^{iq_h^> z}, \quad (8)$$

where the subscripts “ e/h ” of the wave functions denote the electron/hole states, respectively, $\mathbf{q}_{\parallel} = (q_x, q_y)$ is the conserved transverse-wave vector, $\phi = \arctan(\chi q_y/q_x)$, and $\Gamma_{e(h)}^{\pm} = (1 + \chi c \sin \alpha)q_{e(h)}^{\pm} + (-)p_{e(h)}$ with $p_{e(h)} = (E + (-)\mu)/\hbar v_F - (+)\chi q_x c \cos \alpha$. We note that the factor $e^{i\mathbf{q}_{\parallel} \cdot \mathbf{r}_{\parallel}}$ with $\mathbf{r}_{\parallel} = (x, y)$ is omitted in Eq. (8) for simplicity. The longitudinal wave vectors are given by

$$q_{e(h)}^{\pm} = \frac{+(-)\chi p_{e(h)} c \sin \alpha + \zeta_{e(h)} \sqrt{P_{e(h)}^2 - \kappa |\mathbf{q}_{\parallel}|^2}}{\kappa}, \quad (9)$$

where

$$\zeta_{e(h)} = \text{sgn}(p_{e(h)} + \sqrt{\kappa} |\mathbf{q}_{\parallel}|), \quad (10)$$

with $\kappa = 1 - (c \sin \alpha)^2$. Similarly, the scattering states propagating along the $-z$ axis, i.e., $|\varphi^{\lessgtr}\rangle$, can be obtained by the replacement $\zeta_{e(h)} \rightarrow -\zeta_{e(h)}$ in Eqs. (8)–(10).

The requirement for the mean-field treatment of superconductivity is justified in our model as we have taken the heavy-doping limit $|\mu_s| \gg |\mu|$ [42,43] throughout our calculation. In the heavy-doping limit, only the excitations quasiperpendicular transmitting to the superconducting region need to be considered, resulting in the effective excitation gap $\Delta_B = \Delta_0 |\sin \alpha|$ [35,36]. The transmitted states in the superconducting region are given by

$$|\varphi_{s,e}^{\gtrless}\rangle = \begin{pmatrix} \mathcal{P} \\ 0 \\ -\Delta_B \\ 0 \end{pmatrix} e^{iq_{s,e}^{\gtrless} z}, \quad |\varphi_{s,h}^{\gtrless}\rangle = \begin{pmatrix} 0 \\ \Delta_B \\ 0 \\ \mathcal{P} \end{pmatrix} e^{iq_{s,h}^{\gtrless} z}, \quad (11)$$

where $\mathcal{P} = \sqrt{E^2 - \Delta_B^2} + E$ and the subscripts “ e/h ” denote the electronlike/holelike quasiparticle states, respectively. The longitudinal wave vectors in the superconducting region are given by

$$q_{s,e(h)}^{\gtrless} = (\hbar v_F)^{-1} \frac{+(-)\mu_s + \sqrt{E^2 - \Delta_B^2}}{1 - (+)\chi c \sin \alpha}. \quad (12)$$

The total wave function describing the scattering process reads

$$\psi(z) = \begin{cases} |\varphi_e^{\gtrless}\rangle + r|\varphi_e^{\lessgtr}\rangle + r_A|\varphi_h^{\lessgtr}\rangle, & z < 0, \\ t_e|\varphi_{s,e}^{\gtrless}\rangle + t_h|\varphi_{s,h}^{\gtrless}\rangle, & z > 0. \end{cases} \quad (13)$$

Here, $t_{e(h)}$, r and r_A are the transmission amplitude for the electronlike (holelike) state, normal reflection amplitude, and Andreev reflection amplitude, respectively, which can be obtained by matching the wave function at $z = 0$.

The longitudinal conductance for the χ chirality Weyl node is given by the Blonder-Tinkham-Klapwijk approach [44]

$$\sigma_{z,z}^{\chi} = \frac{e^2}{h} \sum_{\mathbf{q}_{\parallel}} (1 + R_A - R), \quad (14)$$

where

$$R_A = \left| \frac{v_{h,z}^{\lessgtr}}{v_{e,z}^{\gtrless}} \right| |r_A|^2, \quad R = \left| \frac{v_{e,z}^{\lessgtr}}{v_{e,z}^{\gtrless}} \right| |r|^2 \quad (15)$$

are the Andreev reflection probability and normal reflection probability, respectively. We note that both r and r_A are the

function of χ . $v_{\zeta,l}^e$ ($\zeta = e, h, \varrho \Rightarrow, <$ and $l = x, y, z$) in Eq. (15) is the group velocity along the l axis for the excitation state $|\varphi_{\zeta}^e\rangle$, which can be obtained by the Hellmann-Feynman theorem [45]:

$$\begin{aligned} v_{\zeta,l}^e &= \frac{\partial E_{\zeta}}{\hbar \partial q_l^e} = \frac{\partial}{\hbar \partial q_l} \langle \varphi_{\zeta}^e | \mathcal{H}_{BdG} | \varphi_{\zeta}^e \rangle \\ &= \hbar^{-1} \langle \varphi_{\zeta}^e | \frac{\partial}{\partial q_l} \mathcal{H}_{BdG} | \varphi_{\zeta}^e \rangle \\ &= \hbar^{-1} \langle \varphi_{\zeta}^e | j_l | \varphi_{\zeta}^e \rangle, \end{aligned} \quad (16)$$

with $j_x = \tau_z(\sigma_x + \chi c \cos \alpha)$, $j_y = -\chi \tau_z \sigma_y$, and $j_z = \tau_z(\sigma_z - \chi c \sin \alpha)$.

The transverse conductance can be calculated within the Landauer formalism [33,46,47] (see Appendix for details)

$$\sigma_{\eta,z}^{\chi} = \frac{e^2}{h} \sum_{\mathbf{q}_{\parallel}} \left(\frac{v_{e,\eta}^{\gtrless}}{v_{e,z}^{\gtrless}} - \frac{v_{e,\eta}^{\lessgtr}}{v_{e,z}^{\lessgtr}} |r|^2 + \frac{v_{h,\eta}^{\lessgtr}}{v_{e,z}^{\lessgtr}} |r_A|^2 \right), \quad (17)$$

where $\eta = \{x, y\}$. The charge Hall angle (ϑ) and the chirality Hall angle (ϑ_{chi}) are given by

$$\tan(\vartheta) = \frac{\sum_{\chi} \sigma_{\eta,z}^{\chi}}{\sum_{\chi} \sigma_{z,z}^{\chi}}, \quad \tan(\vartheta_{\text{chi}}) = \frac{\sum_{\chi} \chi \sigma_{\eta,z}^{\chi}}{\sum_{\chi} \sigma_{z,z}^{\chi}}. \quad (18)$$

III. RESULTS

A. Skew reflection and transverse chirality and charge currents

We first consider the situation where the effective superconducting gap $\Delta_B = \Delta_0 |\sin \alpha|$ is nonzero, i.e., $\alpha \neq 0, \pi$. It is sufficient to consider the normal reflection probability R in the subgap regime ($|E| < \Delta_0 |\sin \alpha|$) on account of $R + R_A = 1$. In the following calculations, we set $\Delta_0 = 1$ meV as the typical experimental value. We focus on the subgap energy regime $|E| < 1$ meV, in which both the normal reflection electrons and the Andreev reflection holes contribute to the transverse chirality Hall current.

The normal reflection probability R versus the incident angle θ_i is shown in Fig. 2(a) for $\alpha = \pi/3$, where the effective superconducting gap is $\Delta_B = 0.86\Delta_0$. Due to the Weyl cones tilt in the q_x - q_z plane in our model, we focus on the reflection in the x - z plane, where the incident angle is given by

$$\theta_i = \arctan \left(\frac{v_{e,x}^{\gtrless}}{v_{e,z}^{\gtrless}} \right). \quad (19)$$

It is shown that the electrons from the $\chi = +1$ chiral node have large reflection probabilities for $-90^\circ < \theta_i < 0^\circ$ [gray line in Fig. 2(a)], which is responsible for the nonzero transverse chirality Hall current. For the electrons from the $\chi = -1$ chiral node, the skew reflection also exists [green line in Fig. 2(a)]. However, the scattering is asymmetric for the electrons from different chiral nodes, i.e., $R_{\chi,\alpha=\pi/3}(\theta_i) \neq R_{-\chi,\alpha=\pi/3}(-\theta_i)$, indicating the presence of a nonzero transverse charge Hall current.

The other two scenarios with $\alpha = -\pi/3$ and $\alpha = 2\pi/3$ are also considered, where the effective superconducting gaps are both $0.86\Delta_0$ as well. The reflection probabilities for $\alpha = -\pi/3$ and $\alpha = 2\pi/3$ are shown in Figs. 2(b) and 2(c), respectively. The chirality-dependent reflection remains present.

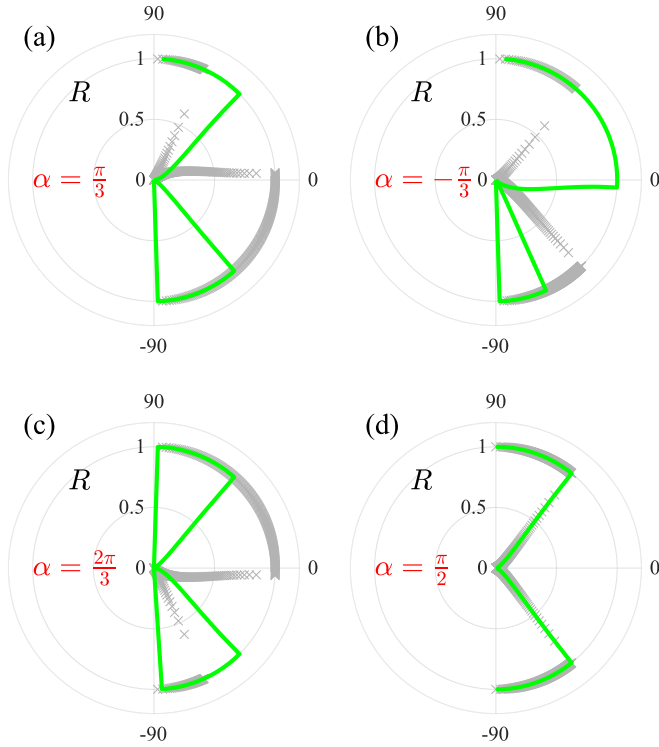


FIG. 2. The reflection probability R versus the incident angle θ_i for $\chi = +1$ (gray) and $\chi = -1$ (green) chiral nodes. Panels (a)-(d) correspond to $\alpha = \pi/3$, $\alpha = -\pi/3$, $\alpha = 2\pi/3$, and $\alpha = \pi/2$, respectively. The other parameters are $c = 0.6$, $E = 0.3\Delta_0$, and $\mu = 1.2\Delta_0$.

However, compared with the $\alpha = \pi/3$ case, the electrons with the opposite (same) chirality are skew reflected to the opposite direction for $\alpha = -\pi/3$ ($2\pi/3$). Consequently, the scattering patterns in Figs. 2(a) and 2(b) are symmetric for different chiralities whereas the scattering patterns in Figs. 2(a) and 2(c) are symmetric for the same chirality.

We note that the Hamiltonian for the tilted Weyl semimetals $\mathcal{H}_\chi = \hbar v_F(\chi c q_i \sigma_0 + q_x \sigma_x + q_z \sigma_z)$ preserves the following symmetries

$$\mathcal{M}\mathcal{H}_\chi(-\alpha, -q_x, q_z)\mathcal{M}^{-1} = \mathcal{H}_{-\chi}(\alpha, q_x, q_z), \quad (20)$$

$$\mathcal{H}_\chi(\pi + \alpha, -q_x, -q_z) = -\mathcal{H}_{-\chi}(\alpha, q_x, q_z), \quad (21)$$

where $\mathcal{M} = \sigma_z$ is the mirror reflection operators about the y - z plane. Equation (20) indicates that under the mirror-reflection symmetry, the Hamiltonian remains unchanged by the substitution $\alpha \rightarrow -\alpha$ and $\chi \rightarrow -\chi$. In the tunneling process, the mirror-reflection symmetry \mathcal{M} reverses the sign of the incident angle, i.e., $\theta_i \rightarrow -\theta_i$. Consequently, the reflection probability holds the relation

$$R_{\chi,\alpha}(\theta_i) = R_{-\chi,-\alpha}(-\theta_i). \quad (22)$$

Similarly, Eq. (21) indicates that the reversal of q_x and q_z results in the reversal of \mathcal{H}_χ by the substitution $\alpha \rightarrow \alpha + \pi$ and $\chi \rightarrow -\chi$. The incident angle remains unchanged in this case. Consequently, the reflection probability holds the relation

$$R_{-\chi,-\alpha}(-\theta_i) = R_{\chi,\pi-\alpha}(-\theta_i) = R_{\chi,\alpha}(\theta_i). \quad (23)$$

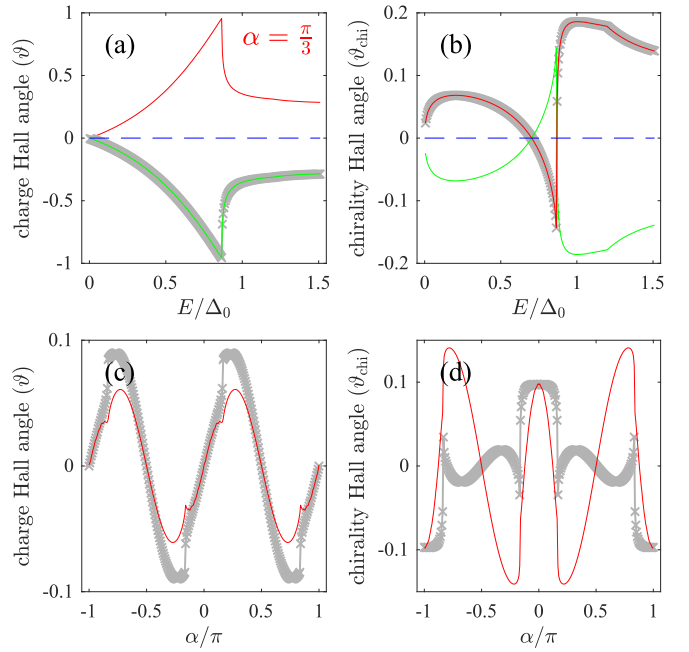


FIG. 3. (a), (b) Charge and chirality Hall angle as a function of the incident energy E for $\alpha = \pi/3$ (red), $\alpha = -\pi/3$ (gray), $\alpha = 2\pi/3$ (green), and $\alpha = \pi/2$ (blue dashed). The other parameters are $c = 0.6$ and $\mu = 1.2\Delta_0$. (c), (d) Charge and chirality Hall angle as a function of α for $\mu = 1.2\Delta_0$ (gray) and $\mu = 0.2\Delta_0$ (red).

For the Andreev reflection probability R_A , the similar identities can be obtained by using the current conservation relation $R_A = 1 - R$.

Consequently, for $\alpha = \pi/3$, the above symmetric relations can be expressed as

$$R_{\chi,\alpha=\pi/3}(\theta_i) = R_{-\chi,\alpha=-\pi/3}(-\theta_i), \quad (24)$$

$$R_{\chi,\alpha=\pi/3}(\theta_i) = R_{\chi,\alpha=2\pi/3}(-\theta_i). \quad (25)$$

For $\alpha = \pi/2$, the skew reflection is absent, and the scattering pattern for $\chi = +1$ and $\chi = -1$ are identical to each other, as shown in Fig. 2(d).

This chirality-dependent skew reflection mentioned above may result in a transverse chirality Hall current as well as a transverse charge Hall current, which can be characterized by the Hall angle. The charge and chirality Hall angles versus the incident energy E at different α are shown in Figs. 3(a) and 3(b), respectively. For $\alpha = \pi/3$, the charge Hall angle ϑ is positive and increases with the increasing of E in the subgap energy regime ($|E| < 0.86\Delta_0$), as shown in Fig. 3(a) (red solid line). However, the chirality Hall angle is not monotonically dependent on E in the subgap regime, as shown in Fig. 3(b) (red solid line). For $\alpha = -\pi/3$ and $2\pi/3$, the charge Hall angles are equal to each other but negative, as the gray and green lines shown in Fig. 3(a), respectively. The chirality Hall angle remains unchanged for $\alpha = -\pi/3$ [gray line in Fig. 3(b)], but reverses its sign for $\alpha = 2\pi/3$ [green line in Fig. 3(b)]. For $\alpha = \pi/2$, both the charge and chirality Hall angle are zero due to the absence of the skew reflection, as shown in Figs. 3(a) and 3(b) (blue dashed lines).

The α dependence of the Hall angle is shown in Figs. 3(c) and 3(d). The charge Hall angle $\vartheta(\alpha)$ is odd parity, as shown in Fig. 3(c), whereas the chirality Hall angle $\vartheta_{\text{chi}}(\alpha)$ is even parity, as shown in Fig. 3(d). It is shown that both ϑ and ϑ_{chi} are absent at $\alpha = \pm\pi/2$. However, for $\alpha = 0$ and π , ϑ_{chi} is finite but $\vartheta = 0$.

With the help of Eqs. (17), (18), and (23), the α -dependent charge and chirality Hall angles can be expressed in terms of R , which are given by

$$\vartheta(\alpha) = \mathcal{Q} \sum_{\chi} \int_{-\pi/2}^{\pi/2} d\theta_i \sin \theta_i R_{\chi}(\theta_i, \alpha), \quad (26)$$

$$\vartheta_{\text{chi}}(\alpha) = \mathcal{Q} \sum_{\chi} \int_{-\pi/2}^{\pi/2} d\theta_i \chi \sin \theta_i R_{\chi}(\theta_i, \alpha), \quad (27)$$

with \mathcal{Q} being a parameter independent of θ_i and $\mathcal{Q}(\alpha) = \mathcal{Q}(-\alpha)$. By substituting Eq. (23) into Eqs. (26) and (27) and changing the integration variable $\theta_i \rightarrow -\theta_i$, one finds

$$\vartheta(\alpha) = -\vartheta(-\alpha) = -\vartheta(\pi - \alpha), \quad (28)$$

$$\vartheta_{\text{chi}}(\alpha) = \vartheta_{\text{chi}}(-\alpha) = -\vartheta_{\text{chi}}(\pi - \alpha), \quad (29)$$

which indicates that the odd-parity charge Hall angle $\vartheta(\alpha)$ disappears at $\alpha = \{\pi/2, -\pi/2, 0, \pi\}$ and the even-parity chirality Hall angle $\vartheta_{\text{chi}}(\alpha)$ disappears at $\alpha = \{\pi/2, -\pi/2\}$.

B. Pure transverse chirality currents

It is noted that the charge Hall angle ϑ vanishes whereas the chirality Hall angle ϑ_{chi} remains finite at $\alpha = \{0, \pi\}$ [see Figs. 3(c) and 3(d)], implying a pure chirality current.

In this scenario the effective pairing potential is zero. Under the heavy-doping condition, the incident electron is local reflected with probability R in the normal region and quasiperpendicular transmitted ($\mathbf{q}_{\parallel} = 0$) as an electronlike quasiparticle with probability $T_e = |v_{s_e, z}^>/v_{e, z}^>||t_e|^2$ in the superconducting region. The current conservation requires $R + T_e = 1$. In the heavy-doping limit $|\mu_s| \gg |\mu|$, the normal reflection probability is only determined by the tilting parameter c . For $\alpha = 0$, the normal reflection probability is obtained analytically as

$$R = \left| \frac{\sqrt{\sec^2 \theta_i - c^2} - 1}{\tan \theta_i - \chi c} \right|^2, \quad (30)$$

where $\theta_i = \arctan(v_{e, x}^>/v_{e, z}^>)$ is the incident angle. For the Weyl node with a given chirality χ , the θ_i -resolved reflection is asymmetric, as shown in Fig. 4(a). The electrons with positive chirality ($\chi = +1$) have large reflection probabilities for $0^\circ < \theta_i < 90^\circ$ (gray lines), whereas the electrons with negative chirality ($\chi = -1$) have large reflection probabilities for $-90^\circ < \theta_i < 0^\circ$ (green lines). The carries with opposite chiralities turn into different transverse directions, leading to a transverse chirality current. With the help of Eqs. (17) and (18), the chirality Hall angle at $\alpha = 0$ is obtained by

$$\tan(\vartheta_{\text{chi}}) = 2 \sin \ell \times \frac{p \cos 2\ell + \cos \ell(\pi \sin \ell - 2)}{\pi \cos 2\ell - 2p \sin 2\ell + 4 \sin \ell}, \quad (31)$$

where $p = \text{arctanh}(\cos \ell)$ with $\ell = \arccos(c)$. The chirality Hall angle is only determined by the tilting parameter c and

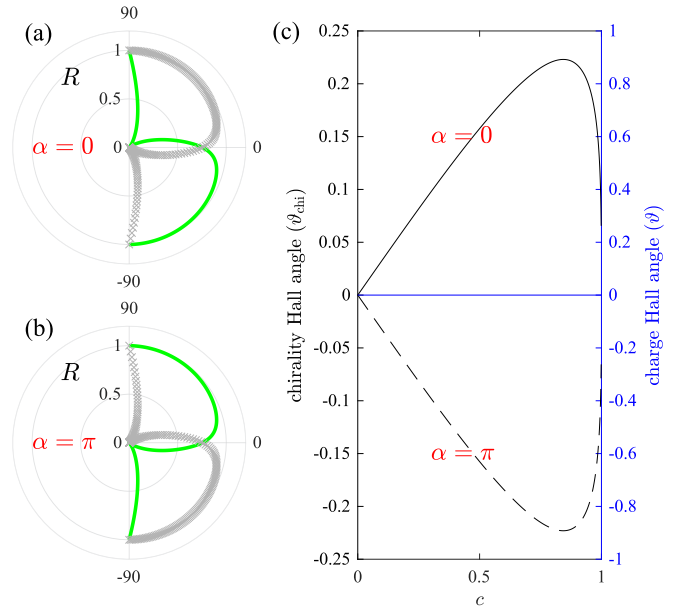


FIG. 4. (a), (b) The reflection probability R versus the incident angle θ_i for $\chi = +1$ (gray) and $\chi = -1$ (green) chiral nodes. (c) Hall angle as a function of the tilting parameter c .

approaches its maximum value at $c \simeq 0.82$ with $\vartheta_{\text{chi}} \simeq 0.22$, as shown in Fig. 4(c) (black solid line). For the nontilting energy dispersion ($c = 0$), the transverse chirality current is absent.

Furthermore, it is found that the scattering pattern is mirror symmetric between two different chiral nodes, i.e.,

$$R_{\chi, \alpha=0}(\theta_i) = R_{-\chi, \alpha=0}(-\theta_i), \quad (32)$$

as shown in Fig. 4(a), leading to a zero net-transverse charge current with

$$\tan(\vartheta) = 0. \quad (33)$$

Consequently, the pure chirality current with zero net charge is predicted for $\alpha = 0$.

For $\alpha = \pi$, the line connecting two opposite chiral Weyl nodes makes a 180° rotation, implying the interchange of the chiralities between the nodes, which leads to the θ_i -resolved $R_{\alpha=\pi}$ being a copy of $R_{\alpha=0}$ with the substitution $\chi \rightarrow -\chi$, as shown in Fig. 4(b). Consequently, the pure transverse chirality Hall current is reversed, while its absolute value remains unchanged, as shown in Fig. 4(c) (black dashed line).

C. Symmetry analysis

Distinct from the Berry curvature-induced Hall effect [48–50], the physical origin of the transverse Hall current in our model is attributed to the symmetry breaking caused by the tilt. The low-energy Hamiltonian for the opposite chiral Weyl nodes at $\pm \mathbf{K}_0$ is given by $\mathcal{H}_{\pm} = \hbar v_F (\pm c q_l \sigma_0 + q_x \sigma_x \mp q_y \sigma_y + q_z \sigma_z)$. For the Weyl cones tilted in q_x - q_z plane, the transverse Hall chirality current and charge current may occur when the angle-resolved reflection is asymmetric for a given chiral node, which requires the tilt breaking the mirror sym-

metry in the $q_y = 0$ plane, i.e.,

$$\mathcal{M}\mathcal{H}_\pm(q_x, q_z)\mathcal{M}^{-1} \neq \mathcal{H}_\pm(-q_x, q_z), \quad (34)$$

where $\mathcal{M} = \sigma_z$ is the mirror-reflection operator about the y - z plane. For $q_t = q_x \cos \alpha - q_z \sin \alpha$, Eq. (34) leads to $\cos \alpha \neq 0$, i.e., $\alpha \neq \pm\pi/2$, which is in agreement with Eqs. (28) and (29).

Furthermore, in order to generate a pure transverse chirality Hall current, the reflection between two different chiral nodes should be symmetric to cancel out the net transverse charge current. This requires an additional \mathbb{Z}_2 exchange symmetry \mathcal{C} [16], which swaps the opposite chiral sector: $\mathcal{C}\mathcal{H}_+(q_x, q_z)\mathcal{C}^{-1} = \mathcal{H}_-(q_x, q_z)$. Consequently, the transverse charge Hall current vanishes when the tilt preserves the combined \mathcal{MC} symmetry

$$(\mathcal{MC})\mathcal{H}_+(q_x, q_z)(\mathcal{MC})^{-1} = \mathcal{H}_-(-q_x, q_z), \quad (35)$$

which results in $\alpha = 0, \pi$.

IV. CONCLUSIONS

To conclude, we study the transverse transport in the NS junctions based on the time-reversal symmetry-broken type-I Weyl semimetals. We focus on the inversion-symmetric tilt, where the two Weyl cones with opposite chiralities have tilts in opposite directions. Our investigation reveals that a chirality-dependent skew reflection occurs at the NS interface due to the tilt of the Weyl cones, resulting in nonzero transverse chirality Hall currents. We further illustrate that the transverse chirality current here is determined by the symmetry of the tilted Weyl Hamiltonian. Specifically, both the transverse chirality Hall current and the transverse charge Hall current may occur when the tilt of the Weyl cones break the mirror symmetry (\mathcal{M}) of the Weyl Hamiltonian. However, a pure transverse chirality Hall current with zero net charge is present when the tilt breaks \mathcal{M} symmetry but preserves the combined \mathcal{MC} symmetry, where \mathcal{C} represents the \mathbb{Z}_2 exchange symmetry. Because the transverse chirality Hall current here is determined by the symmetry of the tilted Weyl Hamiltonian, the results can be generalized to the np junction where the right side of the junction is normal metal and the Andreev reflection is absent. The chirality-dependent skew tunneling still occurs, which is responsible for the transverse chirality currents.

The time-reversal symmetry-broken Weyl semimetals have been proposed theoretically and confirmed experimentally in many realistic systems [51–53]. The proximity-induced superconductivity in Weyl semimetals has been reported both theoretically and experimentally [54–56]. Bachmann *et al.* [57] studied a related Weyl semimetal, niobium arsenide (NbAs), where the electron transport measurements showed superconductivity in the surface layer and provided clear indications of its penetration into the nearby bulk NbAs. The recent experimental paper [58] directly demonstrates the possibility of inducing superconductivity in a type-I Weyl semimetal by coupling niobium phosphide (NbP) surface to a superconductor (Pb, Nb, In).

In addition, the experimental research on the normal metal-superconductor structures performed so far has been done for the tilted Weyl semimetals. The charge transport through the interface between a niobium superconductor and WTe_2 , which

is a typical tilted Weyl semimetal, has been reported [59]. Subsequently, the experimental study on the conductance spectra of (Nb, Pb, In)/NbP superconductor/Weyl semimetal junctions has been reported [58].

The chirality Hall effect leads to the separation and accumulation of left and right chiral fermions on opposite surfaces of the Weyl semimetal-based junction. This chirality polarization results in the unequal optical activity on the opposite surfaces. This manifests as a difference in the absorption of left- and right-handed circularly polarized light at these surfaces. Consequently, the optical activity can be detected via a circular dichroism experiment for the transverse chirality Hall current [13,60]. However, this optical activity is absent for the transverse charge Hall current, which allows it to be distinguished from the chirality Hall current in experiments.

APPENDIX

In this Appendix, we provide the details of the derivation of the transverse conductance and the Hall angle in Eqs. (17) and (18) of the main text.

The transverse current for the given chirality χ along the η axis ($\eta = x, y$) is given by $I_{\chi,\eta} = I_{\chi,\eta}^> + I_{\chi,\eta}^<$ with $I_{\chi,\eta}^>$ ($I_{\chi,\eta}^<$) being the net current flowing from left to right (right to left) [33,44]. In order to get a balanced current in the barrier region, the state propagating towards (outwards) the barrier has a positive (negative) contribution to the transverse current. $I_{\chi,\eta}^>$ is carried by the state $|\varphi^>\rangle = |\varphi_e^>\rangle + r|\varphi_e^<\rangle + r_A|\varphi_h^<\rangle$ with energy E and transverse wave vector \mathbf{q}_\parallel , which is given by

$$\begin{aligned} I_{\chi,\eta}^> &= \frac{e}{L} \sum_{\mathbf{q}_\parallel, q_z} (v_{e,\eta}^> - v_{e,\eta}^< |r|^2) f(E - eV) [1 - f(E)] \\ &\quad - \left(-\frac{e}{L} \right) \sum_{\mathbf{q}_\parallel, q_z} v_{h,\eta}^< |r_A|^2 [1 - f(E + eV)] f(E) \\ &= e \sum_{\mathbf{q}_\parallel} \int \frac{dq_z}{2\pi} [(v_{e,\eta}^> - v_{e,\eta}^< |r|^2) f(E - eV) [1 - f(E)] \\ &\quad + v_{h,\eta}^< |r_A|^2 [1 - f(E + eV)] f(E)] \\ &= \frac{e}{h} \sum_{\mathbf{q}_\parallel} dE \left[\left(\frac{v_{e,\eta}^>}{v_{e,z}^>} - \frac{v_{e,\eta}^<}{v_{e,z}^<} |r|^2 \right) f(E - eV) [1 - f(E)] \right. \\ &\quad \left. + \frac{v_{h,\eta}^<}{v_{e,z}^>} |r_A|^2 [1 - f(E + eV)] f(E) \right]. \quad (\text{A1}) \end{aligned}$$

Here V is the longitudinal voltage drop along the junction and $f(E) = 1/(\exp(E/k_B T) + 1)$ is the Fermi-Dirac distribution function with k_B and T being the Boltzmann constant and temperature, respectively. We note that r , r_A and v in Eq. (A1) are functions of χ , the chirality index χ is omitted here for simplicity.

The net current from right to left ($I_{\chi,\eta}^<$) can be obtained by considering the incoming states in the right superconducting region. Instead of dealing with quasiparticles in the superconducting region, it is equivalent to suppose the incident hole state with energy $-E$ and transverse wave vector $-\mathbf{q}_\parallel$ in the left normal region, i.e., $|\psi^<\rangle = |\psi_h^>\rangle + \bar{r}|\psi_h^<\rangle + \bar{r}_A|\psi_e^<\rangle$, where \bar{r} (\bar{r}_A) is the normal (Andreev) reflection amplitude for

the hole state. Consequently, the net current carried by $|\psi^<\rangle$ reads

$$\begin{aligned} I_{\chi,\eta}^< &= -\frac{e}{L} \sum_{\mathbf{q}_{\parallel}, q_z} \left(v_{h,\eta}^> - v_{e,\eta}^< |\bar{r}|^2 \right) f(-E + eV) [1 - f(-E)] \\ &\quad - \frac{e}{L} \sum_{\mathbf{q}_{\parallel}, q_z} v_{e,\eta}^< |\bar{r}_A|^2 [1 - f(-E - eV)] f(-E) \\ &= -\frac{e}{h} \sum_{\mathbf{q}_{\parallel}} \int dE \left[\left(\frac{v_{h,\eta}^>}{v_{e,z}^>} - \frac{v_{h,\eta}^<}{v_{e,z}^<} |\bar{r}|^2 \right) \right. \end{aligned}$$

$$\times f(-E + eV) [1 - f(-E)]$$

$$\left. + \frac{v_{e,\eta}^<}{v_{h,z}^>} |\bar{r}_A|^2 [1 - f(-E - eV)] f(-E) \right]. \quad (\text{A2})$$

The particle-hole symmetry leads to the following identities

$$\frac{v_{e,\eta}^>}{v_{e,z}^>} = \frac{v_{h,\eta}^>}{v_{h,z}^>}, \quad \frac{v_{e,\eta}^<}{v_{e,z}^<} |r|^2 = \frac{v_{h,\eta}^<}{v_{h,z}^<} |\bar{r}|^2, \quad \frac{v_{h,\eta}^<}{v_{e,z}^<} |r_A|^2 = \frac{v_{e,\eta}^<}{v_{h,z}^<} |\bar{r}_A|^2, \quad (\text{A3})$$

which simplify the expression for the total current

$$\begin{aligned} I_{\chi,\eta} &= I_{\chi,\eta}^> + I_{\chi,\eta}^< \\ &= \frac{e}{h} \sum_{\mathbf{q}_{\parallel}} \int_{-\infty}^{\infty} dE \left(\left[\frac{v_{e,\eta}^>}{v_{e,z}^>} - \frac{v_{e,\eta}^<}{v_{e,z}^<} |r|^2 \right] [f(E - eV) - f(E)] + \frac{v_{h,\eta}^<}{v_{e,z}^<} |r_A|^2 [f(E) - f(E + eV)] \right) \\ &= \frac{e}{h} \sum_{\mathbf{q}_{\parallel}} \int_{-\infty}^{\infty} dE \left(\left[\frac{v_{e,\eta}^>}{v_{e,z}^>} - \frac{v_{e,\eta}^<}{v_{e,z}^<} |r|^2 \right]_{(E)} + \left[\frac{v_{h,\eta}^<}{v_{e,z}^<} |r_A|^2 \right]_{(-E)} \right) [f(E - eV) - f(E)]. \quad (\text{A4}) \end{aligned}$$

Consequently, the transverse conductance is given by

$$\begin{aligned} \sigma_{\eta,z}^{\chi} &= \frac{\partial I_{\chi,\eta}}{\partial V} \\ &= \frac{e^2}{h} \sum_{\mathbf{q}_{\parallel}} \int_{-\infty}^{\infty} dE \left(\left[\frac{v_{e,\eta}^>}{v_{e,z}^>} - \frac{v_{e,\eta}^<}{v_{e,z}^<} |r|^2 \right]_{(E)} + \left[\frac{v_{h,\eta}^<}{v_{e,z}^<} |r_A|^2 \right]_{(-E)} \right) \left[-\frac{\partial(f(E - eV) - f(E))}{\partial(E - eV)} \right] \\ &= \frac{e^2}{h} \sum_{\mathbf{q}_{\parallel}} \int_{-\infty}^{\infty} dE \left(\left[\frac{v_{e,\eta}^>}{v_{e,z}^>} - \frac{v_{e,\eta}^<}{v_{e,z}^<} |r|^2 \right]_{(E)} + \left[\frac{v_{h,\eta}^<}{v_{e,z}^<} |r_A|^2 \right]_{(-E)} \right) \delta(E - eV) \\ &= \frac{e^2}{h} \sum_{\mathbf{q}_{\parallel}} \left(\left[\frac{v_{e,\eta}^>}{v_{e,z}^>} - \frac{v_{e,\eta}^<}{v_{e,z}^<} |r|^2 \right]_{(eV)} + \left[\frac{v_{h,\eta}^<}{v_{e,z}^<} |r_A|^2 \right]_{(-eV)} \right). \quad (\text{A5}) \end{aligned}$$

The longitudinal current can be calculated by the similar method, which reads

$$\begin{aligned} I_{\chi,z} &= I_{\chi,z}^> + I_{\chi,z}^< \\ &= \frac{e}{h} \sum_{\mathbf{q}_{\parallel}} \int_{-\infty}^{\infty} dE \left(\left[1 + \frac{v_{e,z}^<}{v_{e,z}^>} |r|^2 \right] [f(E - eV) - f(E)] - \frac{v_{h,z}^<}{v_{e,z}^<} |r_A|^2 [f(E) - f(E + eV)] \right) \\ &= \frac{e}{h} \sum_{\mathbf{q}_{\parallel}} \int_{-\infty}^{\infty} dE \left(\left[1 + \frac{v_{e,z}^<}{v_{e,z}^>} |r|^2 \right]_{(E)} [f(E - eV) - f(E)] - \left[\frac{v_{h,z}^<}{v_{e,z}^<} |r_A|^2 \right]_{(-E)} [f(E) - f(E + eV)] \right). \quad (\text{A6}) \end{aligned}$$

Consequently, the longitudinal conductance is given by

$$\begin{aligned} \sigma_{z,z}^{\chi} &= \frac{\partial I_{\chi,z}}{\partial V} \\ &= \frac{e^2}{h} \sum_{\mathbf{q}_{\parallel}} \int_{-\infty}^{\infty} dE \left(\left[1 + \frac{v_{e,z}^<}{v_{e,z}^>} |r|^2 \right]_{(E)} - \left[\frac{v_{h,z}^<}{v_{e,z}^<} |r_A|^2 \right]_{(-E)} \right) \left[-\frac{\partial(f(E - eV) - f(E))}{\partial(E - eV)} \right] \\ &= \frac{e^2}{h} \sum_{\mathbf{q}_{\parallel}} \int_{-\infty}^{\infty} dE \left(\left[1 + \frac{v_{e,z}^<}{v_{e,z}^>} |r|^2 \right]_{(E)} - \left[\frac{v_{h,z}^<}{v_{e,z}^<} |r_A|^2 \right]_{(-E)} \right) \delta(E - eV) \\ &= \frac{e^2}{h} \sum_{\mathbf{q}_{\parallel}} \left(1 + \left[\frac{v_{e,z}^<}{v_{e,z}^>} |r|^2 \right]_{(eV)} - \left[\frac{v_{h,z}^<}{v_{e,z}^<} |r_A|^2 \right]_{(-eV)} \right). \quad (\text{A7}) \end{aligned}$$

It is noted that, for the incident (reflected) states, the longitudinal group velocities are always positive (negative), i.e., $v_{e,z}^> < 0$ and $v_{e/h,z}^< < 0$. However, the sign of the transverse group velocity is uncertain. Consequently, for the longitudinal conductance, the reflection coefficients can be written as

$$\frac{v_{e,z}^<}{v_{e,z}^>} |r|^2 = - \left| \frac{v_{e,z}^<}{v_{e,z}^>} \right| |r|^2 = -R, \quad (\text{A8})$$

$$\frac{v_{h,z}^<}{v_{e,z}^>} |r_A|^2 = - \left| \frac{v_{h,z}^<}{v_{e,z}^>} \right| |r_A|^2 = -R_A, \quad (\text{A9})$$

where R_A (R) is positive and denotes the reflection probability for the Andreev reflection (normal reflection). In the subgap

regime, $A + B = 1$ due to the current conservation. The longitudinal conductance [Eq. (A7)] can be expressed in terms of R and R_A :

$$\sigma_{z,z}^{\chi} = \frac{e^2}{h} \sum_{\mathbf{q}_{\parallel}} (1 - R + R_A), \quad (\text{A10})$$

which is the Blonder-Tinkham-Klapwijk formalism. The charge Hall angle (ϑ) and the chirality Hall angle (ϑ_{chi}) are given by

$$\tan(\vartheta) = \frac{\sum_{\chi} \sigma_{\eta,z}^{\chi}}{\sum_{\chi} \sigma_{z,z}^{\chi}}, \quad \tan(\vartheta_{\text{chi}}) = \frac{\sum_{\chi} \chi \sigma_{\eta,z}^{\chi}}{\sum_{\chi} \sigma_{z,z}^{\chi}}. \quad (\text{A11})$$

-
- [1] N. P. Armitage, E. J. Mele, and A. Vishwanath, Weyl and Dirac semimetals in three-dimensional solids, *Rev. Mod. Phys.* **90**, 015001 (2018).
- [2] X. Wan, A. M. Turner, A. Vishwanath, and S. Y. Savrasov, Topological semimetal and Fermi-arc surface states in the electronic structure of pyrochlore iridates, *Phys. Rev. B* **83**, 205101 (2011).
- [3] C.-K. Chan, N. H. Lindner, G. Refael, and P. A. Lee, Photocurrents in Weyl semimetals, *Phys. Rev. B* **95**, 041104(R) (2017).
- [4] H. B. Nielsen and M. Ninomiya, Absence of neutrinos on a lattice:(II). Intuitive topological proof, *Nucl. Phys. B* **193**, 173 (1981).
- [5] A. A. Burkov and L. Balents, Weyl semimetal in a topological insulator multilayer, *Phys. Rev. Lett.* **107**, 127205 (2011).
- [6] H. Weng, C. Fang, Z. Fang, B. A. Bernevig, and X. Dai, Weyl semimetal phase in noncentrosymmetric transition-metal monophosphides, *Phys. Rev. X* **5**, 011029 (2015).
- [7] Q. Chen, F. Chen, Y. Pan, C. Cui, Q. Yan, L. Zhang, Z. Gao, S. A. Yang, Z.-M. Yu, H. Chen *et al.*, Discovery of a maximally charged Weyl point, *Nat. Commun.* **13**, 7359 (2022).
- [8] G. Chang, B. J. Wieder, F. Schindler, D. S. Sanchez, I. Belopolski, S.-M. Huang, B. Singh, D. Wu, T.-R. Chang, T. Neupert *et al.*, Topological quantum properties of chiral crystals, *Nat. Mater.* **17**, 978 (2018).
- [9] A. A. Zyuzin and A. A. Burkov, Topological response in Weyl semimetals and the chiral anomaly, *Phys. Rev. B* **86**, 115133 (2012).
- [10] A. Burkov, Chiral anomaly and transport in Weyl metals, *J. Phys.: Condens. Matter* **27**, 113201 (2015).
- [11] J. Xiong, S. K. Kushwaha, T. Liang, J. W. Krizan, M. Hirschberger, W. Wang, R. J. Cava, and N. P. Ong, Evidence for the chiral anomaly in the Dirac semimetal Na_3Bi , *Science* **350**, 413 (2015).
- [12] S. A. Yang, H. Pan, and F. Zhang, Chirality-dependent Hall effect in Weyl semimetals, *Phys. Rev. Lett.* **115**, 156603 (2015).
- [13] S. Ghosh, D. Sinha, S. Nandy, and A. Taraphder, Chirality-dependent planar Hall effect in inhomogeneous Weyl semimetals, *Phys. Rev. B* **102**, 121105(R) (2020).
- [14] B. Jiang, L. Wang, R. Bi, J. Fan, J. Zhao, D. Yu, Z. Li, and X. Wu, Chirality-dependent Hall effect and antisymmetric magnetoresistance in a magnetic Weyl semimetal, *Phys. Rev. Lett.* **126**, 236601 (2021).
- [15] S.-B. Zhang, J. Erdmenger, and B. Trauzettel, Chirality Josephson current due to a novel quantum anomaly in inversion-asymmetric Weyl semimetals, *Phys. Rev. Lett.* **121**, 226604 (2018).
- [16] D. Sinha, Anomalous Josephson effect and quantum anomaly in inversion asymmetric Weyl semimetals, *Phys. Rev. B* **103**, 125147 (2021).
- [17] S. A. Jafari, Electric field assisted amplification of magnetic fields in tilted Dirac cone systems, *Phys. Rev. B* **100**, 045144 (2019).
- [18] M. O. Goerbig, J.-N. Fuchs, G. Montambaux, and F. Piéchon, Tilted anisotropic Dirac cones in quinoid-type graphene and α -(BEDT-TTF) $_2\text{I}_3$, *Phys. Rev. B* **78**, 045415 (2008).
- [19] D. C. Cabra, N. E. Grandi, G. A. Silva, and M. B. Sturla, Low-energy electron-phonon effective action from symmetry analysis, *Phys. Rev. B* **88**, 045126 (2013).
- [20] Y. Mao, W. L. Wang, D. Wei, E. Kaxiras, and J. G. Soderstri, Graphene structures at an extreme degree of buckling, *ACS Nano* **5**, 1395 (2011).
- [21] P. Li, Y. Wen, X. He, Q. Zhang, C. Xia, Z.-M. Yu, S. A. Yang, Z. Zhu, H. N. Alshareef, and X.-X. Zhang, Evidence for topological type-II Weyl semimetal WTe_2 , *Nat. Commun.* **8**, 2150 (2017).
- [22] A. A. Soluyanov, D. Gresch, Z. Wang, Q. Wu, M. Troyer, X. Dai, and B. A. Bernevig, Type-II Weyl semimetals, *Nature (London)* **527**, 495 (2015).
- [23] B. Q. Lv, H. M. Weng, B. B. Fu, X. P. Wang, H. Miao, J. Ma, P. Richard, X. C. Huang, L. X. Zhao, G. F. Chen, Z. Fang, X. Dai, T. Qian, and H. Ding, Experimental discovery of Weyl semimetal TaAs, *Phys. Rev. X* **5**, 031013 (2015).
- [24] S.-Y. Xu, N. Alidoust, I. Belopolski, Z. Yuan, G. Bian, T.-R. Chang, H. Zheng, V. N. Strocov, D. S. Sanchez, G. Chang *et al.*, Discovery of a Weyl fermion state with Fermi arcs in niobium arsenide, *Nat. Phys.* **11**, 748 (2015).
- [25] Z.-M. Yu, Y. Yao, and S. A. Yang, Predicted unusual magnetoresistance in type-II Weyl semimetals, *Phys. Rev. Lett.* **117**, 077202 (2016).
- [26] J. Ma, Q. Gu, Y. Liu, J. Lai, P. Yu, X. Zhuo, Z. Liu, J.-H. Chen, J. Feng, and D. Sun, Nonlinear photoresponse of type-II Weyl semimetals, *Nat. Mater.* **18**, 476 (2019).
- [27] Y. Ferreiros, A. A. Zyuzin, and J. H. Bardarson, Anomalous nernst and thermal Hall effects in tilted Weyl semimetals, *Phys. Rev. B* **96**, 115202 (2017).

- [28] Z. Hou and Q.-F. Sun, Double Andreev reflections in type-II Weyl semimetal-superconductor junctions, *Phys. Rev. B* **96**, 155305 (2017).
- [29] D. Sinha, Josephson effect in type-I Weyl semimetals, *Phys. Rev. B* **102**, 085144 (2020).
- [30] K. Das and A. Agarwal, Linear magnetochiral transport in tilted type-I and type-II Weyl semimetals, *Phys. Rev. B* **99**, 085405 (2019).
- [31] S.-H. Zhang, D.-F. Shao, Z.-A. Wang, J. Yang, W. Yang, and E. Y. Tsymbal, Tunneling valley Hall effect driven by tilted Dirac fermions, *Phys. Rev. Lett.* **131**, 246301 (2023).
- [32] K. Das, K. Ghorai, D. Culcer, and A. Agarwal, Nonlinear valley Hall effect, *Phys. Rev. Lett.* **132**, 096302 (2024).
- [33] S. Datta, *Electronic Transport in Mesoscopic Systems* (Cambridge University Press, Cambridge, 1995).
- [34] W. Chen, L. Jiang, R. Shen, L. Sheng, B. Wang, and D. Xing, Specular Andreev reflection in inversion-symmetric Weyl semimetals, *Europhys. Lett.* **103**, 27006 (2013).
- [35] K. A. Madsen, E. J. Bergholtz, and P. W. Brouwer, Josephson effect in a Weyl SNS junction, *Phys. Rev. B* **95**, 064511 (2017).
- [36] D. Breunig, S.-B. Zhang, M. Stehno, and B. Trauzettel, Influence of a chiral chemical potential on Weyl hybrid junctions, *Phys. Rev. B* **99**, 174501 (2019).
- [37] G. Bednik, A. A. Zyuzin, and A. A. Burkov, Superconductivity in Weyl metals, *Phys. Rev. B* **92**, 035153 (2015).
- [38] A. Volkov, P. Magnée, B. Van Wees, and T. Klapwijk, Proximity and Josephson effects in superconductor-two-dimensional electron gas planar junctions, *Physica C: Superconductivity* **242**, 261 (1995).
- [39] C. W. J. Beenakker, Specular Andreev reflection in graphene, *Phys. Rev. Lett.* **97**, 067007 (2006).
- [40] W. Zeng and R. Shen, Pure crossed Andreev reflection assisted transverse valley currents in $\alpha - \mathcal{T}_3$ lattices, *Phys. Rev. B* **106**, 094503 (2022).
- [41] P.-G. Gennes, *Superconductivity of Metals and Alloys* (CRC, Boca Raton, FL, 2018).
- [42] C. W. J. Beenakker, Colloquium: Andreev reflection and Klein tunneling in graphene, *Rev. Mod. Phys.* **80**, 1337 (2008).
- [43] W. Zeng and R. Shen, Enhanced Andreev reflection in Kekulé-Y patterned graphene, *Phys. Rev. B* **104**, 075436 (2021).
- [44] A. Matos-Abiague and J. Fabian, Tunneling anomalous and spin Hall effects, *Phys. Rev. Lett.* **115**, 056602 (2015).
- [45] R. P. Feynman, Forces in molecules, *Phys. Rev.* **56**, 340 (1939).
- [46] D. C. Langreth and E. Abrahams, Derivation of the Landauer conductance formula, *Phys. Rev. B* **24**, 2978 (1981).
- [47] P. F. Bagwell and T. P. Orlando, Landauer's conductance formula and its generalization to finite voltages, *Phys. Rev. B* **40**, 1456 (1989).
- [48] K. F. Mak, K. L. McGill, J. Park, and P. L. McEuen, The valley Hall effect in MoS₂ transistors, *Science* **344**, 1489 (2014).
- [49] A. F. Young, C. R. Dean, L. Wang, H. Ren, P. Cadden-Zimansky, K. Watanabe, T. Taniguchi, J. Hone, K. L. Shepard, and P. Kim, Spin and valley quantum Hall ferromagnetism in graphene, *Nat. Phys.* **8**, 550 (2012).
- [50] J. Liu, Z. Ma, J. Gao, and X. Dai, Quantum valley Hall effect, orbital magnetism, and anomalous Hall effect in twisted multi-layer graphene systems, *Phys. Rev. X* **9**, 031021 (2019).
- [51] M. Hirschberger, S. Kushwaha, Z. Wang, Q. Gibson, S. Liang, C. A. Belvin, B. A. Bernevig, R. J. Cava, and N. P. Ong, The chiral anomaly and thermopower of Weyl fermions in the half-heusler GdPtBi, *Nat. Mater.* **15**, 1161 (2016).
- [52] K. Kuroda, T. Tomita, M.-T. Suzuki, C. Bareille, A. Nugroho, P. Goswami, M. Ochi, M. Ikhlas, M. Nakayama, S. Akebi *et al.*, Evidence for magnetic Weyl fermions in a correlated metal, *Nat. Mater.* **16**, 1090 (2017).
- [53] A. Sakai, Y. P. Mizuta, A. A. Nugroho, R. Sihombing, T. Koretsune, M.-T. Suzuki, N. Takemori, R. Ishii, D. Nishio-Hamane, R. Arita *et al.*, Giant anomalous nernst effect and quantum-critical scaling in a ferromagnetic semimetal, *Nat. Phys.* **14**, 1119 (2018).
- [54] T. Meng and L. Balents, Weyl superconductors, *Phys. Rev. B* **86**, 054504 (2012).
- [55] U. Khanna, A. Kundu, S. Pradhan, and S. Rao, Proximity-induced superconductivity in Weyl semimetals, *Phys. Rev. B* **90**, 195430 (2014).
- [56] Q. Li, C. He, Y. Wang, E. Liu, M. Wang, Y. Wang, J. Zeng, Z. Ma, T. Cao, C. Yi *et al.*, Proximity-induced superconductivity with subgap anomaly in type II Weyl semi-metal WTe₂, *Nano Lett.* **18**, 7962 (2018).
- [57] M. D. Bachmann, N. Nair, F. Flicker, R. Ilan, T. Meng, N. J. Ghimire, E. D. Bauer, F. Ronning, J. G. Analytis, and P. J. Moll, Inducing superconductivity in Weyl semimetal microstructures by selective ion sputtering, *Sci. Adv.* **3**, e1602983 (2017).
- [58] G. Grabecki, A. Dąbrowski, P. Iwanowski, A. Hruban, B. J. Kowalski, N. Olszowska, J. Kołodziej, M. Chojnacki, K. Dybko, A. Łusakowski, T. Wojtowicz, T. Wojciechowski, R. Jakiela, and A. Wiśniewski, Conductance spectra of (Nb, Pb, In)/NbP superconductor/Weyl semimetal junctions, *Phys. Rev. B* **101**, 085113 (2020).
- [59] A. Kononov, O. O. Shvetsov, S. V. Egorov, A. V. Timonina, N. N. Kolesnikov, and E. V. Deviatov, Signature of Fermi arc surface states in Andreev reflection at the WTe₂ Weyl semimetal surface, *Europhys. Lett.* **122**, 27004 (2018).
- [60] P. Hosur and X.-L. Qi, Tunable circular dichroism due to the chiral anomaly in Weyl semimetals, *Phys. Rev. B* **91**, 081106(R) (2015).